RGD Peptide–Conjugated Multimodal NaGdF$_4$:Yb^{3+}/Er^{3+} Nanophosphors for Upconversion Luminescence, MR, and PET Imaging of Tumor Angiogenesis

Junghan Lee, Tae Sup Lee, Jiyoung Ryu, Sukmin Hong, Moonsik Kang, Kangbin Im, Joo Hyun Kang, Sang Moo Lim, Sun Park and Rita Song

This article and updated information are available at:
http://jnm.snmjournals.org/content/54/1/96

Information about reproducing figures, tables, or other portions of this article can be found online at:
http://jnm.snmjournals.org/site/misc/permission.xhtml

Information about subscriptions to JNM can be found at:
http://jnm.snmjournals.org/site/subscriptions/online.xhtml

RGD Peptide–Conjugated Multimodal NaGdF$_4$:Yb^{3+}/Er^{3+} Nanophosphors for Upconversion Luminescence, MR, and PET Imaging of Tumor Angiogenesis

Junghan Lee*[1], Tae Sup Lee*[2], Jiyoung Ryu[1], Sukmin Hong[1], Moonsik Kang[3], Kangbin Im[3], Joo Hyun Kang[2], Sang Moo Lim[2], Sun Park[4], and Rita Song[1]

[1]Nano/Bio Chemistry Laboratory, Institut Pasteur Korea, Gyeonggi-do, South Korea; [2]Molecular Imaging Research Center, Korea Institute of Radiological and Medical Science, Seoul, South Korea; [3]Applied Microscope Laboratory, Institut Pasteur Korea, Gyeonggi-do, South Korea; and [4]Department of Microbiology, Ajou University School of Medicine, Gyeonggi-do, South Korea

Multimodal nanoparticles have been extensively studied for target-specific imaging and therapy of various diseases, including cancer. In this study, radiolabeled arginine-glycine-aspartic acid (RGD)–functionalized Er^{3+}/Yb^{3+} co-doped NaGdF$_4$ upconversion nanophosphors (UCNPs) were synthesized and evaluated as a multimodal PET/MR/optical probe with tumor angiogenesis–specific targeting properties. **Methods:** A dimeric cyclic RGDyk ((cRGDyk)$_2$) peptide was conjugated to polyacrylic acid–coated NaGdF$_4$:Yb^{3+}/Er^{3+} UCNPs along with polyethylene glycol molecules and was consecutively radiolabeled with ^{124}I. In vitro cytotoxicity testing was performed for 3 d. Upconversion luminescence imaging of (cRGDyk)$_2$-UCNP was performed on U87MG cells with a laboratory-made confocal microscope. In vivo small-animal PET and clinical 3-T T1-weighted MR imaging of ^{124}I-labeled RGD–functionalized UCNPs was acquired with or without blocking of cyclic RGD peptide in a U87MG tumor model. Inductively coupled plasma mass spectrometry and biologic transmission electron microscopy were done to evaluate gadolinium concentration and UCNP localization, respectively. **Results:** Polymer-coated UCNPs and dimeric RGD–conjugated UCNPs were monodispersely synthesized, and those of hydrodynamic size were 30 ± 8 nm and 32 ± 9 nm, respectively. (cRGDyk)$_2$-UCNPs have a low cytotoxic effect on cells. Upconversion luminescence signals of (cRGDyk)$_2$-UCNP were specifically localized on the surface of U87MG cells. ^{124}I-c(RGDyk)$_2$-UCNPs specifically accumulated in U87MG tumors (2.8 ± 0.8 vs. 1.3 ± 0.4 percentage injected dose per gram in the blocking experiment), and T1-weighted MR images showed significant positive contrast enhancement in U87MG tumors. Tumor localization of ^{124}I-c(RGDyk)$_2$-UCNPs was confirmed by inductively coupled plasma mass spectrometry and biologic transmission electron microscopy analysis. **Conclusion:** These results suggest that ^{124}I-labeled RGD–functionalized UCNPs have high specificity for $\alpha_v\beta_3$ integrin–expressing U87MG tumor cells and xenografted tumor models. Multimodal UCNPs can be used as a platform nanoparticle with multimodal imaging for cancer-specific diagnoses.

$\mathbf{M}$olecular imaging using nanoparticles has been widely applied because of its great potential for early detection, accurate diagnosis, and targeted therapy of various diseases, especially cancer (1,2). The development of multimodal probes has been brought about by the great progress in the development of multimodal imaging instruments such as PET/MR, PET/CT, and SPECT/CT (3–6). Multimodal imaging probes provide several advantages, such as administration of a single contrast agent for different types of imaging modalities, and signal consistency at the target region without the difference in biodistribution that may occur when more than 2 kinds of contrast agent are used.

Application of near-infrared–emitting dyes for in vivo imaging has been of great interest because of their advantageous optical properties, such as low phototoxicity, deep penetration, and no autofluorescence (7–10). In particular, near-infrared nanoparticles have been known to exhibit high photostability and versatile surface modification—properties superior to those of organic dyes.

Upconversion nanophosphors (UCNPs) with the composition of NaYF$_4$:Yb^{3+}/Er^{3+} have recently been reported to be potential candidates for in vivo imaging probes using a 980-nm laser (11,12). Their unique optical property occurs via an upconversion process in which 2 photons are sequentially absorbed to emit fluorescence of a high level of energy (13). The replacement of Y with Gd in NaYF$_4$:Yb^{3+}/Er^{3+} has been known to offer special magnetic properties in addition to the fluorescence, thus having potential for use in optical and MR imaging. In a previous study, we reported facile synthesis of small, hexagonal NaGdF$_4$:Yb^{3+}/X^{3+} (X = Er or Tm) UCNPs and their magnetic resonance and optical characteristics (14). Some UCNPs labeled with radionuclide also showed potential

for use as trimodality in vivo imaging probes for PET/MR/optical imaging (15).

Angiogenesis-targeting arginine-glycine-aspartic acid (RGD) peptide has been widely used to detect the angiogenesis of cancer (16,17). RGD peptide has been known to specifically bind to integrin $\alpha_v\beta_3$, which is overexpressed on both tumor and vasculature in many cancer types. RGD peptide–coupled nanoparticles were extensively studied in cancer-specific targeted imaging using quantum dots (18), iron oxide nanoparticles (4,19), and UCNPs (20).

In this study, highly qualified $NaGdF_4$:Yb^{3+}/Er^{3+} UCNPs were synthesized and evaluated as a trimodal upconversion PET/MR/luminescence probe with specific tumor angiogenesis–targeting properties. A dimeric cyclic RGDyk ((cRDGyk)$_2$) peptide was conjugated to $NaGdF_4$:Yb^{3+}/Er^{3+} UCNP along with optimized polyethylene glycol (PEG) molecules and was consecutively radiolabeled with ^{124}I using a tyrosine residue of (cRGDyk)$_2$ peptide (Fig. 1). Our multimodal UCNPs were evaluated in cell cultures and in living mice bearing U87MG human glioblastoma tumors to investigate the feasibility of multimodal imaging using cancer targeting to $\alpha_v\beta_3$ integrin.

MATERIALS AND METHODS

Reagents

Lanthanide chloride ($LnCl_3$, Ln = Gd, Yb, and Er, 99.99%), sodium trifluoroacetate (98%), 1-octadecene (90%), oleic acid (90%), tetramethyl-ammonium hydroxide, N-(3-dimethylaminopropyl)-N′-ethylcarbodiimide hydrochloride (EDC), polyacrylic acid (molecular weight, 1,800), octylamine (99%), and dimethylsulfoxide were purchased from Aldrich. All chemicals were of analytic grade and used without further purification. N-hydroxysulfosuccinimide was purchased from Fluka, and methoxypolyethylene glycol amine (molecular weight, 2,000) was obtained from Sunbio. (cRGDyk)$_2$ (H-Glu(Arg-Gly-Asp-D-Tyr-Lys)$_2$, where H is the hydrogen of the N-terminal and D is an optical isomer) was purchased from Peptides International, and Dulbecco modified Eagle medium, fetal bovine serum, penicillin–streptomycin, and phosphate-buffered saline (pH 7.4) were obtained from Gibco. The human glioblastoma U87MG cell line was purchased from American Type Culture Collection. Paraformaldehyde and Iodo-Beads were purchased from Wako and Pierce, respectively.

Preparation of (cRGDyk)$_2$-UCNP Conjugates

$NaGdF_4$:Yb^{3+}/Er^{3+} UCNP was synthesized according to a method reported in the literature (14). Briefly, $GdCl_3$ (0.8 mmol), $YbCl_3$ (0.18 mmol), and $ErCl_3$ (0.02 mmol) in a mixture of oleic acid (6 mL) and 1-octadecene (15 mL) were reacted under a vacuum at 120°C for 1 h. Sodium trifluoroacetate (2.5 mmol) was added at room temperature, and the mixture was heated to 300°C under an N_2 flow for 2 h to yield UCNPs. The synthesized UCNPs were redispersed in toluene. UCNPs capped with oleic acid/1-octadecene were further water-solubilized by surface coating using an amphophilic polymer, octylamine-modified polyacrylic acid. The solution of UCNPs was added dropwise to the polymer (20 mg) solution in chloroform and vigorously stirred. After the reaction, the chloroform was evaporated to yield a thin film of the polymer-coated UCNPs, and distilled water was added. An aqueous solution of polymer-coated UCNPs was finally purified by gel permeability chromatography, using 0.05 M sodium borate buffer (pH 8.5) as the eluent and an ultraviolet detector at 254 nm.

(cRGDyk)$_2$-UCNP conjugates were synthesized by a coupling reaction of the carboxyl and amine group of the UCNP and (cRGDyk)$_2$, respectively (18,21). At the same time, PEG molecules were introduced on the UCNPs to improve stability and reduce uptake by the reticuloendothelial system. One hundred microliters of polymer-coated UCNPs (1 μM, 10.7 mg/mL) were activated by an excess amount of EDC (500 nmol) and N-hydroxysulfosuccinimide (125 nmol) for 30 min, and the excess of the activation reagents was removed by membrane filtration (molecular weight cutoff, 30 kDa).
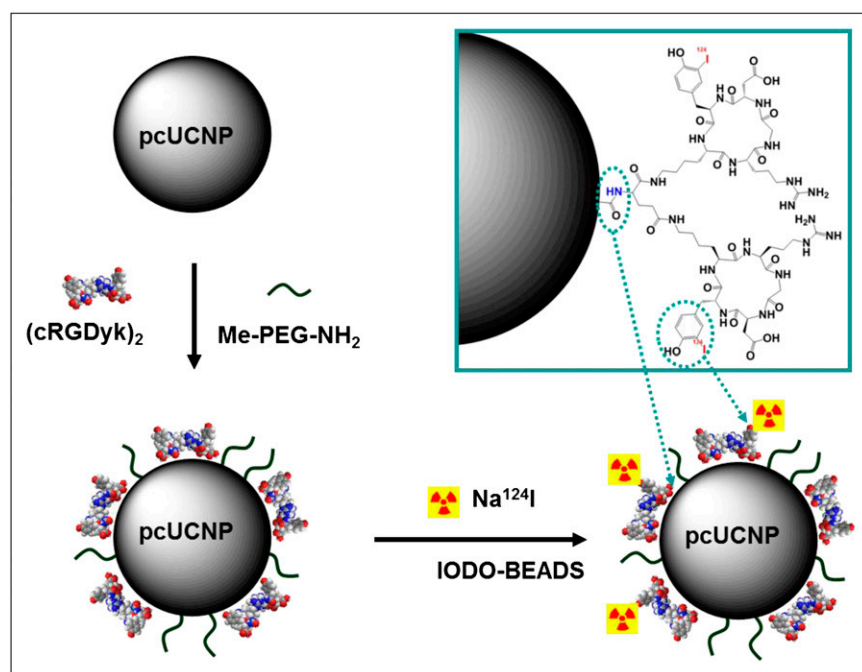
FIGURE 1. Synthesis scheme of ^{124}I-(cRGDyk)$_2$-UCNP conjugates. Polymer-coated UCNP (pcUCNP) was reacted both with (cRGDyk)$_2$ peptide and with MeO-PEG-NH$_2$ (molecular weight, 2,000) using EDC/N-hydroxysulfosuccinimide. Tyrosine residue of (cRGDyk)$_2$ was labeled with ^{124}I using Iodo-Beads (Pierce).

N-hydroxysuccinimide–activated UCNPs were added to the mixture of $(cRGDyk)_2$ peptide and methoxypolyethylene glycol amine (peptide:PEG = 1,000:0, 800:200, 500:500, 200:8,000, and 0:1,000) and reacted for 3 h. The progress and completion of the reaction were confirmed by gel electrophoresis. The unreacted excess of $(cRGDyk)_2$ and PEG was removed by membrane filtration (molecular weight cutoff, 30 kDa).

Characterization of UCNPs and (cRGDyk)$_2$–UCNP Conjugates

The size distribution and morphology of synthesized NaGdF4: Yb^{3+}/Er^{3+} UCNPs were analyzed by scanning transmission electron microscopy (CM-30; Philips) and x-ray diffractometry (XPERT XPD; Philips). All absorption spectra were obtained in a quartz cuvette using a Cary 5000 ultraviolet–visible spectrometer (Varian Inc.). Photoluminescence was measured by a Fluorolog-3 spectrofluorimeter (Horiba Jobin Yvon) with excitation at 980 nm at an integration time of 0.1 s. Agarose gel electrophoresis was performed using 1% agarose in 0.5× tris-borate ethylenediamine tetraacetic acid buffer (pH 8.0) at 50 V·cm^{-1} for 40 min. The resulting gel image was obtained on an LAS 3000 gel imager (Fuji). For identification of UCNPs, the gel was poststained with SYBR green (Invitrogen). For the hydrodynamic size measurement of the $(cRGDyk)_2$ UCNP conjugates, dynamic light scattering analysis was performed using Nano-ZS (Malvern) at room temperature. Polymer-coated UCNPs were purified by gel permeation chromatography equipped with a Delta 600 controller, a model 2487 ultraviolet detector, and an automatic fraction collector (Waters Co.).

Upconversion Luminescence Imaging

The U87MG human glioblastoma cells were maintained at 37°C in a humidified atmosphere containing 5% CO_2 in Dulbecco modified Eagle medium supplemented with 10% fetal bovine serum and 1% penicillin–streptomycin. U87MG cells (40,000 cells per well) were seeded in a glass-bottomed 8-well chamber slide (Lab-Tek) with 400 μL of culture medium. After cell growth in 5% CO_2 at 37°C for 24 h, $(cRGDyk)_2$-UCNP conjugates (final concentration, 0.2 μM) were added into the cell solution and incubated at 4°C for 2 h. The cells were then washed 3 times with fresh phosphate-buffered saline and fixed with 4% paraformaldehyde for 10 min. As a control experiment, the cells were preincubated with 500 μM $(cRGDyk)_2$ at 4°C for 1 h to block integrin $\alpha_v\beta_3$ receptor. The fluorescence images were obtained by a confocal microscope built in our laboratory for specific use in studying the optical properties of upconversion nanoparticles (excitation wavelength, 980 nm; emission filter, ~540–560 nm) (22).

Cytotoxicity

For determining the cytotoxicity of UCNPs, a methylthiazol-tetrazolium assay was performed. U87MG cells were incubated with various concentrations of UCNPs in a dose-dependent manner for 18 and 72 h. U87MG cells (2×10^3 per well) were seeded on 96-well plates and placed in a complete growth medium (Dulbecco modified Eagle medium with 10% fetal bovine serum) in a 5% CO_2 incubator at 37°C. UCNPs ranging from about 0 to 200 μg/mL were then added to each well. After incubation for 18 or 72 h, the percentage of viable cells was assayed using methylthiazol-tetrazolium. At each time point, methylthiazol-tetrazolium (0.5 mg/mL, Sigma) was added to each well, and the plates were incubated at 37°C for 4 h. The methylthiazol-tetrazolium solution was then replaced with dimethylsulfoxide to dissolve the formazan crystal product formed by the viable cells. Spectrophotometric data were obtained by measuring the absorbance using a Victor 3 microplate reader (Perkin Elmer).

Radiolabeling of (cRGDyk)$_2$-UCNPs with ^{124}I

$(cRGDyk)_2$-UCNPs was radiolabeled with ^{124}I using a method previously reported (23). Briefly, $(cRGDyk)_2$-UCNP (10 mg) and Na^{124}I (46 MBq) produced by a MC-50 cyclotron (Korea Institute of Radiological and Medical Sciences) were mixed with activated Iodo-Beads and reacted for 1 h. ^{124}I-labeled $(cRGDyk)_2$-UCNP was purified by membrane filtration (molecular weight cutoff, 10 kDa; NanoSep). Radiolabeling yield and purity were analyzed using instant thin-layer chromatography silica gel as the stationary phase and saline as the mobile phase.

Xenograft Tumor Model

Six- to 8-wk-old athymic BALB/c mice that weighed 20–24 g and were from a specific-pathogen-free breeding colony were purchased from Orient Bio. U87MG cells were harvested using 0.05% trypsin–ethylenediamine tetraacetic acid, centrifuged, and resuspended in sterile phosphate-buffered saline as a final cell concentration of $1 \times 10^6/0.05$ mL, which was injected into the right shoulder region of the mice. The T1-weighted contrast effect has been known to be barely visible in a small tumor. Therefore, to show the potential of the new material as an MR contrast agent, in vivo imaging experiments were conducted when the tumors reached about 1–2 cm in length, allowing us to maximize the contrast-to-noise ratio on T1-weighted MR images. All animal experiments were conducted with the approval of the Institutional Animal Care and Use Committee.

In Vivo MR imaging

To image tumor angiogenesis in the $\alpha_v\beta_3$-expressing U87MG tumor–bearing mice (n = 3/group), we injected into the tail vein ^{124}I-$(cRGDyk)_2$-UCNPs (1.66 MBq/2 mg) or ^{124}I-$(cRGDyk)_2$-UCNPs (1.66 MBq/2 mg) after a blocking dose of $(cRGDyk)_2$ (10 mg/kg). Using a T1-weighted sequence (repetition time, 637 ms; echo time, 12 ms; flip angle, 180; matrix, 256×152; and slice thickness, 1.0 mm) and a wrist coil, MR imaging was performed on a 3-T Magnetom Trio (Siemens) before contrast administration and 0.5, 1, 4 h after contrast administration. MR coronal and transverse cross-section images were obtained for each animal. Using Syngo software (Siemens Medical Systems), signal intensities were measured in defined regions of interest that were in locations similar to the tumor center.

In Vivo Small-Animal PET

Tumor imaging with ^{124}I-$(cRGDyk)_2$-UCNP in the U87MG tumor model was performed using a small-animal PET system (Inveon; Siemens Medical Systems). The small-animal PET scan was acquired immediately after MR imaging. ^{124}I-$(cRGDyk)_2$-UCNPs (1.66 MBq/2 mg) or ^{124}I-$(cRGDyk)_2$-UCNPs (1.66 MBq/2 mg) were injected into the mice after a blocking dose of $(cRGDyk)_2$ (10 mg/kg). The mice were scanned for a 60-min static image. PET data analyses were performed in list-mode acquisition and subsequently presented as a histogram in a single frame. Images were reconstructed using 2-dimensional ordered-subset expectation maximization and ramp filter algorithms supplied by Inveon Acquisition Workplace software. Images were visualized using Inveon Research Workplace software. Small-animal PET images were presented as the percentage injected dose per gram (%ID/g), which was calculated as region-of-interest activity divided by injected dose (24).

Tissue Analysis by Inductively Coupled Plasma Mass Spectrometry (ICP-MS) and Biologic Transmission Emission Microscopy (TEM)

The U87MG tumor–bearing mice were sacrificed immediately after completion of the PET scan. For confirmation of UCNP in liver and tumor tissue, Gd^{3+} content was determined by ICP-MS analysis (ELAN6100 DRC; PerkinElmer, Korea Institute of Science and Technology). Liver and tumor tissues were dissolved in c-HNO_3 solution before ICP-MS analysis. The distribution of UCNP in each tissue was also observed by biologic TEM analysis (Tecnai G2 Spirit, 120 kV; FEI Co., Korea Basic Science Institute). Extracted tissues were immerged in liquid nitrogen and sectioned at a thickness of 1 μm using a cryostat. Each sample was then stained with 3% uranyl acetate and lead citrate for 20 and 15 min, respectively, before TEM analysis.

Statistical Analysis

Each reported value represents the mean ± SD. Differences between groups were tested for statistical significance using the Student t test. A P value of less than 0.05 was considered significant.

RESULTS

Synthesis and Characterization of UCNPs

$NaGdF_4$:Yb^{3+}/Er^{3+} UCNP was synthesized by thermolysis of lanthanide chloride and sodium trifluoroacetic acid at high temperature (>250°C) in a mixture of oleic acid and 1-octadecene. The obtained UCNPs were small and highly monodispersed, showing a β-phase hexagonal structure. The crystal structure of the $NaGdF_4$:Yb^{3+}/Er^{3+} UCNP obtained from the reaction performed in the solvent mixture of oleic acid and 1-octadecene (1:1) at 300°C was analyzed by TEM, selected area electron diffraction, and x-ray diffractometry. Figure 2A shows a representative TEM bright-field image of the $NaGdF_4$:Yb^{3+}/Er^{3+} UCNPs, which are of uniform spheric shape with a diameter of 24 ± 1.5 nm. The high-resolution TEM image presented in Figure 2B shows a lattice distance of 0.532 nm, corresponding to d spacing for the (100) lattice plane in the hexagonal $NaGdF_4$ structure. Figure 2C shows the typical emission and excitation spectra of the $NaGdF_4$:Yb^{3+}/Er^{3+} UCNP. The conventional quantum yield

FIGURE 2. (A) TEM bright-field image. (B) High-resolution TEM image of $NaGdF_4$:Yb^{3+}/Er^{3+} and selected area electron diffraction pattern (inset). (C) Emission spectra (green) and ultraviolet–visible spectra (black) of $NaGdF_4$:Yb^{3+}/Er^{3+} and upconversion luminescence of UCNP in toluene under excitation of 980-nm laser (inset). a.u. = arbitrary units.

measurement is based on the ratio of relative fluorescent fluorophores at the same concentration. However, the unknown extinction coefficient value (ε) of UCNPs did not allow calculation of the exact quantum yield. The photostability of as-synthesized UCNPs was investigated under continuous laser excitation at 980 nm with a power density of 500 mW/cm^3 and was found to be unchanged for 2 h.

Water solubilization was performed by the polymer-coating method using amphophilic poly(acrylic acid) derivatives modified with 40% octylamine. The strong upconversion luminescence and magnetic properties were maintained after polymer coating and purification by gel permeability chromatography. Polymer-coated UCNP contains carboxylic acid functionality, which was used further for the conjugation reaction.

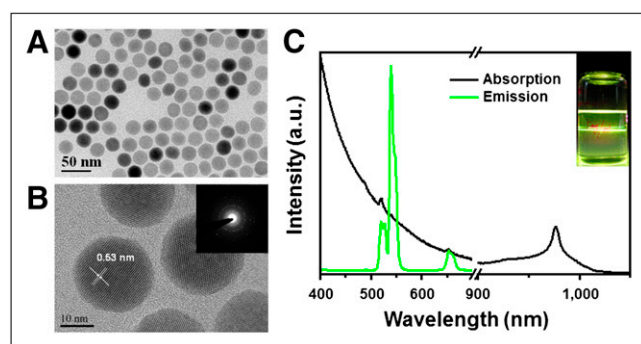### Synthesis and Characterization of (cRGDyk)$_2$-UCNP Conjugates

The reaction mixture composed of different ratios of PEG/(cRGDyk)$_2$ was added to the aqueous solution of UCNPs in the presence of EDC and N-hydroxysulfosuccinimide. As shown in Figure 3A, the conjugation with both PEG and (cRGDyk)$_2$ peptide showed a delayed gel migration pattern due to the increased molecular weight and decreased negative charges. The conjugation reaction was optimized with 1:200:800 UCNP:(cRGDyk)$_2$:PEG. The stability of as-synthesized UCNPs was tested by incubation in phosphate-buffered saline for 24 h at room temperature as shown as in Figure 3B (Supplemental Figs. 1A and 1B). The UCNP that was conjugated with a high ratio of PEG exhibited good stability for 24 h at room temperature, without any noticeable aggregates. The hydrodynamic size of pegylated (cRGDyk)$_2$-UCNPs was measured by dynamic light scattering and found to be 32 ± 9 nm (Fig. 3C).

Upconversion Luminescence Imaging

Live cell–labeling experiments using (cRGDyk)$_2$-UCNPs were performed before in vivo imaging to confirm the specificity for integrin $\alpha_\nu\beta_3$ in vitro. The fluorescence microscope was built in our laboratory to be adapted for upconversion luminescence (*14*). Figures 4A and 4B show specific binding of (cRGDyk)$_2$-UCNP conjugates to cell surface integrin $\alpha_\nu\beta_3$ of U87MG cells. At the same time, a blocking experiment was also performed as a control experiment. U87MG cells were pretreated with an excess amount of free (cRGDyk)$_2$ peptide (500 μM) and then incubated with (cRGDyk)$_2$-UCNP conjugates. This experiment confirmed that the binding of (cRGDyk)$_2$-UCNP conjugates was receptor-specific, given that it was completely inhibited under the condition in which integrin $\alpha_\nu\beta_3$ was saturated with free (cRGDyk)$_2$ peptide.

Cytotoxicity

The in vitro toxicity of as-synthesized UCNPs was investigated in the U87MG cell line. Notable cytotoxicity below a 50 μg/mL concentration of UCNP was not observed after

FIGURE 3. (A) Gel electrophoresis image of (cRGDyk)$_2$-UCNP conjugates with various ratios of PEG to peptide: lane a, polymer-coated UCNP; lane b, (cRGDyk)$_2$-UCNP without PEG (UCNP:(cRGDyk)$_2$ = 1:1,000); lanes c, d, and e, UCNP:(cRGDyk)$_2$:PEG = 1:800:200, 1:500:500, and 1:200:800, respectively; lane f, pegylated UCNP without (cRGDyk)$_2$ (UCNP:PEG = 1:1,000). Gel condition: 1% agarose gel, 0.5× TBE buffer (pH 8.5), 50 V·cm^{-1}, 40 min. Gel image was obtained by SYBR green (Invitrogen) staining. (B) Stability of nanoparticles incubated in 1× phosphate-buffered saline for 24 h at room temperature. (C) Hydrodynamic size of UCNPs measured by dynamic light scattering (polymer-coated UCNP [pcUCNP], 30 ± 8 nm [black]; (cRGDyk)$_2$-UCNP [UCNP:(cRGDyk)$_2$:PEG = 1:200:800], 32 ± 9 nm) [red]).
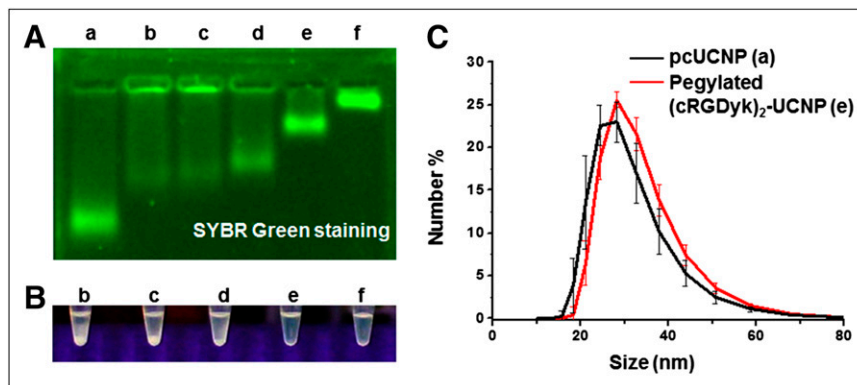
72 h of incubation. Viability above a 100–200 μg/mL concentration of UCNP was slightly decreased (Fig. 4C), but the difference was not statistically significant.

Radiolabeling of (cRGDyk)$_2$-UCNPs with ^{124}I

(cRGDyk)$_2$-UCNPs were then labeled with Na^{124}I (46 MBq) using Iodo-Beads in sodium phosphate buffer (pH 7.5). ^{124}I, a PET radionuclide, was directly conjugated to the tyrosine residue of (cRGDyk)$_2$ bound to UCNP. The radiolabeling yield was approximately 19%, and specific radioactivity was estimated to be approximately 0.88 GBq/g. There was no aggregate or precipitate of nanoparticles during the radiolabeling and purification procedures.

In Vivo MR imaging

The integrin $\alpha_v\beta_3$–targeting ability of ^{124}I-(cRGDyk)$_2$-UCNPs was investigated using in vivo T1-weighted MR imaging of U87MG tumor–bearing nude mice (Fig. 5A). At 4 h after injection of ^{124}I-(cRGDyk)$_2$-UCNPs, the MR signal intensity of the tumor region was significantly increased. ^{124}I-(cRGDyk)$_2$-UCNPs also showed a high accumulation in liver due to the inherent size effect of nanoparticles engulfed by the major rough reticuloendothelial system. The signal-to-noise ratio of U87MG tumors was determined as the ratio of tumor intensity before injection of ^{124}I-(cRGDyk)$_2$-UCNPs to the tumor intensity afterward. The signal-to-noise ratio of U87MG tumors at 4 h was 1.8 ± 0.1 times higher than that on non–contrast-enhanced MR images of mice injected with ^{124}I-(cRGDyk)$_2$-UCNP. The signal-to-noise ratio of liver also increased—by

2.3 ± 0.1-fold—compared with that on unenhanced T1-weighted MR images. However, there was no statistical difference between the signal-to-noise ratio of tumor tissue before injection and the ratio after injection in mice in which integrin $\alpha_v\beta_3$ was blocked by an excess of (cRGDyk)$_2$ peptide.

In Vivo Small-Animal PET

After T1-weighted MR imaging, the integrin $\alpha_v\beta_3$–targeting ability of ^{124}I-(cRGDyk)$_2$-UCNPs with small-animal PET was determined at 1 and 4.5 h after injection in U87MG tumor–bearing nude mice. Representative coronal and transverse PET images were obtained of U87MG tumor–bearing mice at 4.5 h after injection of ^{124}I-(cRGDyk)$_2$-UCNPs. U87MG tumors were clearly visualized by specific binding (Supplemental Fig. 5; supplemental materials are available online at http://jnm.snmjournals.org). In region-of-interest analysis, uptake of ^{124}I-(cRGDyk)$_2$-UCNPs in U87MG tumors without and with blocking peptide–injected mice was 2.8 ± 0.8 %ID/g and 1.3 ± 0.4 %ID/g, respectively (Fig. 5B). Administration of ^{124}I-(cRGDyk)$_2$-UCNPs with pretreatment blocking (cRGDyk)$_2$ peptide revealed a significantly reduced uptake in tumor tissue. MR images showed high uptake of radiolabeled nanoparticles (26.0 ± 1.4 %ID/g at 4.5 h) in the liver. In the control experiment, injection of radiolabeled UCNPs with blocking (cRGDyk)$_2$ peptide showed minimal uptake in U87MG tumors. There was no significant difference in the image-based biodistribution between mice injected with ^{124}I-(cRGDyk)$_2$-UCNPs and mice

FIGURE 4. Upconversion luminescence image of U87MG cells and cytotoxicity test. (A) Image of U87MG cells incubated with (cRGDyk)$_2$-UCNP. (B) Image of U87MG cells incubated with (cRGDyk)$_2$-UCNP after pretreatment with excess of (cRGDyk)$_2$ peptide. (C) Methylthiazol-tetrazolium assay cell proliferation assay.
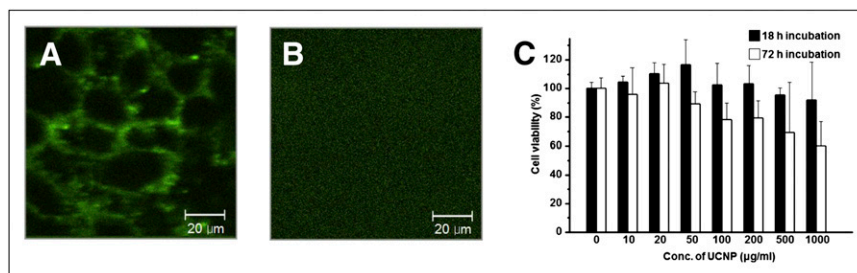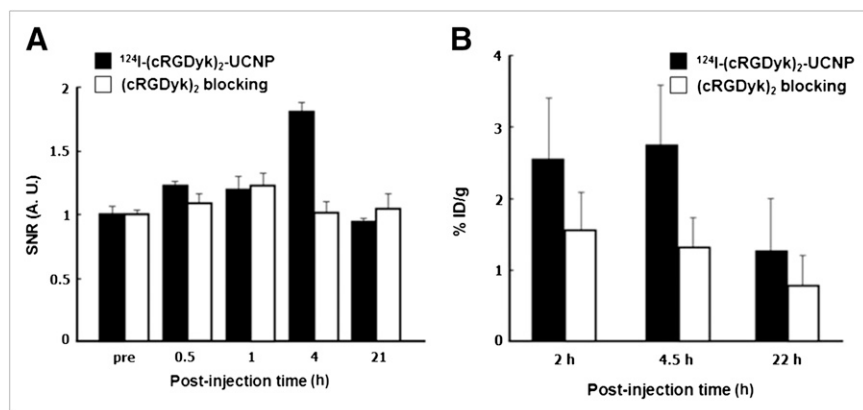
FIGURE 5. (A) Time-dependent signal-to-noise ratio (SNR) change in ^{124}I-(cRGDyk)$_2$-UCNPs with or without blocking dose of (cRGDyk)$_2$ peptide. (B) Time-dependent % ID/g change in ^{124}I-(cRGDyk)$_2$-UCNPs with or without blocking dose of (cRGDyk)$_2$ peptide. A. U. = 5 arbitrary units.

injected with cyclic RGD preblocking ^{124}I-(cRGDyk)$_2$-UCNPs (Supplemental Figs. 4A and 4B, respectively), except for kidney uptake at 2 h after injection. ^{124}I-(cRGDyk)$_2$-UCNPs showed high uptake in the liver and spleen. Most ^{124}I-(cRGDyk)$_2$-UCNPs accumulated in the reticuloendothelial system. On comparison of the images of 2 modalities, radiolabeled nanoparticles showed positive contrast in the central region of U87MG tumors on MR images (Supplemental Fig. 5A), and that region matched with hot spots on PET images (Supplemental Fig. 5B).

Tissue Analysis by ICP-MS and Biologic TEM

After MR and PET imaging, the liver and tumor tissues of each mouse were excised and fixed with 4% paraformaldehyde. The presence of rare earth metal in the nanoparticles facilitates quantitative analysis of UCNP in the tissues, and the concentration of Gd^{3+} in liver and tumor tissue was directly analyzed by means of ICP-MS. For comparison, the tissues that were excised from the mice in the blocking experiment were also analyzed. The most significant value was obtained when the concentration of Gd^{3+} in tumor (0.12 ppm) was compared with that of the blocking experiment (0.067 ppm). The concentration of the (cRGDyk)$_2$-conjugated UCNP for the tumor tissue was determined to be twice as high, which is highly consistent with the in vivo result obtained in both MR and PET experiments. The concentration of UCNP in the liver (38 ppm) is much higher than that in any other organ.

Confirmation of the MR and PET results was obtained from biologic TEM analysis of the same excised tissues. Figure 6 shows TEM images of tumor tissues without and with blocking by (cRGDyk)$_2$ peptides. Some UCNPs were found in the tumor tissue but were barely seen in the blocking experiment. Abundantly embedded UCNPs were found in liver tissue, as was consistent with the results obtained by ICP-MS analysis, MR, and PET (data not shown).

DISCUSSION

We have demonstrated an RGD-functionalized trimodal nanoparticle for in vivo target-specific upconversion luminescence imaging, T1-weighted contrast-enhanced MR imaging, and PET imaging of tumors based on $\alpha_v\beta_3$ integrin.

Recently, RGD-coupled dual-modality nanoparticles such as iron oxide nanoparticles with radioisotopes (4), fluorescent dye–conjugated silica nanoparticles with radioisotopes (19), and gold nanoparticles with radioisotopes (20,25) have been used for tumor-specific imaging. Dual-modality imaging with nanoparticles can provide high-spatial-resolution anatomic information and quantitative information to target concentration. Our multifunctional nanoparticles can provide not only gadolinium-based high-resolution MR images and ^{124}I-based quantitative PET images but also intraoperative detection and imaging of nodal metastases using upconversion luminescence due to low background fluorescence.

This study, although demonstrating multimodal imaging of RGD-functionalized UCNPs for targeting tumor angiogenesis, was limited in that it lacked an instrument for in vivo imaging and thus could not provide in vivo upconversion luminescence images. However, our RGD-functionalized UCNPs were visualized by background-free optical imaging of the surface of U87MG cells with near-infrared (980 nm) excitation (Fig. 4A). Our synthesized NaGdF4: Yb^{3+}/Er^{3+} UCNPs had a hexagonal structure that has been reported to show much higher fluorescent efficiency than does a cubic structure (26–28). Upconversion luminescence was found to be extremely resistant to photobleaching, and
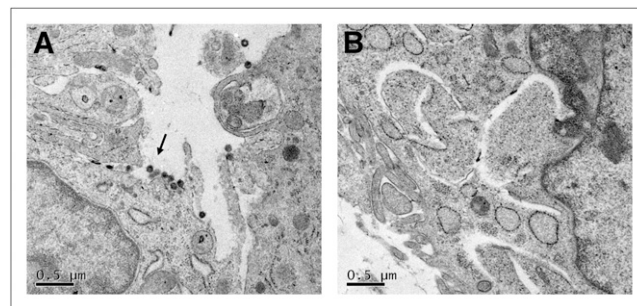
FIGURE 6. Biologic TEM images of U87MG tumor tissues. (A) Tumor tissue injected with ^{124}I-(cRGDyk)$_2$-UCNPs (1.66 MBq/2 mg). (B) Tumor tissue injected with ^{124}I-(cRGDyk)$_2$-UCNP (1.66 MBq/2 mg) after blocking with excess amount of (cRGDyk)$_2$ peptide (10 mg/kg). Frozen tumor section (1-μm thickness) was stained with 3% uranyl acetate for 20 min and lead citrate for 15 min. Arrow: UCNPs.

no photoblinking occurred. In contrast to conventional fluorescence imaging, upconversion luminescence has several advantages such as a high signal-to-noise ratio, high detection sensitivity because of no autofluorescence, deep tissue penetration by the noninvasive near-infrared excitation, and low photodamage to living organisms (27).

RGD-functionalized UCNPs showed low cytotoxicity in vitro (Fig. 4C). However, we did not determine in vivo toxicity in our UCNPs. In vivo toxicity needs careful histologic and metabolic investigation. In our study, apparent cytotoxicity was not observed, and the mice had a lengthy survival, even after injection of 2 mg per mouse in the preliminary study.

Radiolabeled $(cRGDyk)_2$-UCNPs gave positive-contrast T1-weighted MR images and small-animal PET images of U87MG tumors (Figs. 5A and 6A), as confirmed by ICP-MS and biologic TEM analysis. In PET and MR images and gadolinium concentration analysis, the uptake of radiolabeled $(cRGDyk)_2$-UCNPs in U87MG tumors was approximately 2-fold higher than that in U87MG tumors given preblocking free cyclic RGD dimer. In previous reports (4,19), RGD-conjugated nanoparticles showed maximum tumor uptake at early time points. ^{64}Cu-labeled RGD-functionalized iron oxide nanoparticles showed peak uptake at 4 h (~10 %ID/g) (4) or 6 h (~5 %ID/g) (19) in tumors. Compared with the previous studies, our RGD-functionalized UCNPs showed relatively low uptake (~2.8 %ID/g at 4.5 h) in U87MG tumors. In another study, ^{124}I-labeled RGD-functionalized silica nanoparticles showed similarly low uptake (~2 %ID/g at 4 h) in tumors (29). The low uptake may be caused by deiodination of radioiodine from radioiodinated cyclic RGD.

Accumulation of radiolabeled $(cRGDyk)_2$-UCNPs mainly in the liver reticuloendothelial system has been considered a general observation for all kinds of nanoparticles because of their inherent size effect. We used PEG to prevent accumulation in the reticuloendothelial system. The PEG molecule has been widely used in biology, pharmaceutics, and polymer chemistry to avoid nonspecific binding and to improve the target-specific properties (30). In our case, UCNP that had been conjugated together with the PEG molecule and $(cRGDyk)_2$ peptide showed good target specificity. However, further strategies to prevent accumulation in the reticuloendothelial system of the liver will be needed to improve the specific targeting of nanoparticles.

CONCLUSION

$NaGdF_4$:Yb^{3+}/Er^{3+} UCNPs with interesting dual-modality optical and magnetic properties were synthesized and labeled with ^{124}I for use as a trimodal imaging probe, that is, MR/PET/optical. In addition, tumor targeting was achieved by conjugation with cyclic RGD peptide. The tumor-specific binding properties of RGD-conjugated UCNP were visualized through in vitro upconversion luminescence microscopy of U87MG cells. Both T1-weighted MR and PET using ^{124}I-

$(cRGDyk)_2$-UCNP showed clear tumor targeting. This imaging result was further confirmed by ICP-MS and biologic TEM analysis of tumor tissues. Three different imaging modalities and one functional targeting property were successfully realized in a single UCNP, which shows great potential to be an easy-to-use and sensitive imaging probe for cancer-specific diagnosis.

DISCLOSURE

REFERENCES

1. Gunasekera UA, Pankhurst QA, Douek M. Imaging applications of nanotechnology in cancer. *Target Oncol.* 2009;4:169–181.

2. Louie A. Multimodality imaging probes: design and challenges. *Chem Rev.* 2010;110:3146–3195.

3. Choi JS, Park JC, Nah H, et al. A hybrid nanoparticle probe for dual-modality positron emission tomography and magnetic resonance imaging. *Angew Chem Int Ed Engl.* 2008;47:6259–6262.

4. Lee HY, Li Z, Chen K, et al. PET/MRI dual-modality tumor imaging using arginine-glycine-aspartic (RGD)-conjugated radiolabeled iron oxide nanoparticles. *J Nucl Med.* 2008;49:1371–1379.

5. Pichler BJ, Wehrl HF, Kolb A, Judenhofer MS. Positron emission tomography/magnetic resonance imaging: the next generation of multimodality imaging? *Semin Nucl Med.* 2008;38:199–208.

6. Xie H, Wang ZJ, Bao A, Goins B, Phillips WT. In vivo PET imaging and biodistribution of radiolabeled gold nanoshells in rats with tumor xenografts. *Int J Pharm.* 2010;395:324–330.

7. Yi G, Chow G. Synthesis of hexagonal-phase NaYF4:Yb,Er and NaYF4:Yb,Tm nanocrystals with efficient up-conversion fluorescence. *Adv Funct Mater.* 2006;16:2324–2329.

8. Mai HX, Zhang YW, Sun LD, Yan CH. Highly efficient multicolor up-conversion emissions and their mechanisms of monodisperse NaYF$_4$:Yb,Er core and core/shell-structured nanocrystals. *J Phys Chem C.* 2007;111:13721–13729.

9. Wang F, Liu X. Recent advances in the chemistry of lanthanide-doped upconversion nanocrystals. *Chem Soc Rev.* 2009;38:976–989.

10. Cheng L, Yang K, Zhang S, Shao M, Lee S, Liu Z. Highly-sensitive multiplexed in vivo imaging using pegylated upconversion nanoparticles. *Nano Res.* 2010;3:722–732.

11. Yu XF, Sun Z, Li M, et al. Neurotoxin-conjugated upconversion nanoprobes for direct visualization of tumors under near-infrared irradiation. *Biomaterials.* 2010;31:8724–8731.

12. Cheng L, Yang K, Shao M, Lee S, Liu Z. Multicolor in vivo imaging of upconversion nanoparticles with emissions tuned by luminescence resonance energy transfer. *J Phys Chem C.* 2011;115:2686–2692.

13. Boyer JC, Cuccia LA, Capobianco JA. Synthesis of colloidal up converting NaYF4:Er^{3+}/Yb^{3+} and Tm^{3+}/Yb^{3+} monodisperse nanocrystals. *Nano Lett.* 2007;7:847–852.

14. Ryu J, Park HY, Kim K, et al. Facile synthesis of ultrasmall and hexagonal NaGdF4: Yb^{3+}, Er^{3+} nanoparticles with magnetic and upconversion imaging properties. *J Phys Chem C.* 2010;114:21077–21082.

15. Zhou J, Yu M, Sun Y, et al. Fluorine-18-labeled Gd^{3+}/Yb^{3+}/Er^{3+} co-doped NaYF4 nanophosphors for multimodality PET/MR/UCL imaging. *Biomaterials.* 2011;32:1148–1156.

16. Buckley CD, Pilling D, Henriquez NV, et al. RGD peptides induce apoptosis by direct caspase-3 activation. *Nature.* 1999;397:534–539.

17. Desgrosellier JS, Cheresh DA. Integrins in cancer: biological implications and therapeutic opportunities. *Nat Rev Cancer.* 2010;10:9–22.

18. Cai W, Shin DW, Chen K, et al. Peptide-labeled near-infrared quantum dots for imaging tumor vasculature in living subjects. *Nano Lett.* 2006;6:669–676.

19. Benezra M, Penate-Medina O, Zanzonico PB, et al. Multimodal silica nanoparticles are effective cancer-targeted probes in a model of human melanoma. *J Clin Invest.* 2011;121:2768–2780.

20. Kim YH, Jeon J, Hong SH, et al. Tumor targeting and imaging using cyclic RGD-PEGylated gold nanoparticle probes with directly conjugated iodine-125. *Small.* 2011;7:2052–2060.

21. Li ZB, Cai W, Cao Q, et al. ^{64}Cu-labeled tetrameric and octameric RGD peptides for small-animal PET of tumor $\alpha_v\beta_3$ integrin expression. *J Nucl Med.* 2007; 48:1162–1171.

22. Im KB, Kang MS, Kim J, et al. Two-photon spectral imaging with high temporal and spectral resolution. *Opt Express.* 2010;18:26905–26914.

23. Kim JH, Lee JS, Lee TS, Park H, Chun KS. Optimization studies on the production of high-purity [124]I using (p,2n) reaction. *J Labelled Comp Radiopharm.* 2007;50:511–512.

24. Woo SK, Lee TS, Kim KM, et al. Anesthesia condition for ^{18}F-FDG imaging of lung metastasis tumors using small animal PET. *Nucl Med Biol.* 2008;35: 143–150.

25. Morales-Avila E, Ferro-Flores G, Ocampo-García BE, et al. Multimeric system of ^{99m}Tc-labeled gold nanoparticles conjugated to c[RGDfK(C)] for molecular imaging of tumor $\alpha_{v\beta3}$ expression. *Bioconjug Chem.* 2011;22:913–922.

26. Guo H, Li Z, Qian H, Hu Y, Muhammad IN. Seed-mediated synthesis of NaYF$_4$: Yb, Er/NaGdF$_4$ nanocrystals with improved upconversion fluorescence and MR relaxivity. *Nanotechnology.* 2010;21:125602–125608.

27. Park YI, Kim JH, Lee KT, et al. Nonblinking and nonbleaching upconverting nanoparticles as an optical imaging nanoprobe and T1 magnetic resonance imaging contrast agent. *Adv Funct Mater.* 2009;21:4467–4471.

28. Vetrone F, Naccache R, Mahalingam V, Morgan CG, Capobianco JA. The active-core/active-shell approach: a strategy to enhance the upconversion luminescence in lanthanide-doped nanoparticles. *Adv Funct Mater.* 2009;19:2924–2929.

29. Yang X, Hong H, Grailer JJ, et al. cRGD-functionalized, DOX-conjugated, and ^{64}Cu-labeled superparamagnetic iron oxide nanoparticles for targeted anticancer drug delivery and PET/MR imaging. *Biomaterials.* 2011;32:4151–4160.

30. Otsuka H, Nagasaki Y, Kataoka K. PEGylated nanoparticles for biological and pharmaceutical applications. *Adv Drug Deliv Rev.* 2003;55:403–419.